ACS Photonics

Article

pubs.acs.org/journal/apchd5

Controlling Metamaterial Transparency with Superchiral Fields

Christopher Kelly,*[,†] Larousse Khosravi Khorashad,[‡] Nikolaj Gadegaard,[§] Laurence D. Barron,[†] Alexander O. Govorov,[‡] Affar S. Karimullah,*[,†,§] and Malcolm Kadodwala*[,†]

[†]School of Chemistry, Joseph Black Building, University of Glasgow, Glasgow, G12 8QQ, United Kingdom

[‡]Department of Physics and Astronomy, Ohio University, Athens, Ohio 45701, United States

[§]School of Engineering, Rankine Building, University of Glasgow, Glasgow, G12 8LT, United Kingdom

Supporting Information

ABSTRACT: The advent of metamaterials has heralded a period of unprecedented control of light. The optical responses of metamaterials are determined by the properties of constituent nanostructures. The current design philosophy for tailoring metamaterial functionality is to use geometry to control the nearfield coupling of the elements of the nanostructures. A drawback of this geometry-focused strategy is that the functionality of a metamaterial is predetermined and cannot be manipulated easily postfabrication. Here we present a new design paradigm for metamaterials, in which the coupling between chiral elements of a nanostructure is controlled by the chiral asymmetries of the nearfield, which can be externally manipulated. We call this mechanism dichroic coupling. This phenomenon is used to control the electromagnetic induced transparency displayed by a chiral metamaterial by tuning the chirality of the near fields. This "non-geometric" paradigm for controlling optical properties offers the opportunity to optimally design chiral metamaterials for applications in the polarization state control and for ultrasensitive analysis of biomaterials and soft matter.

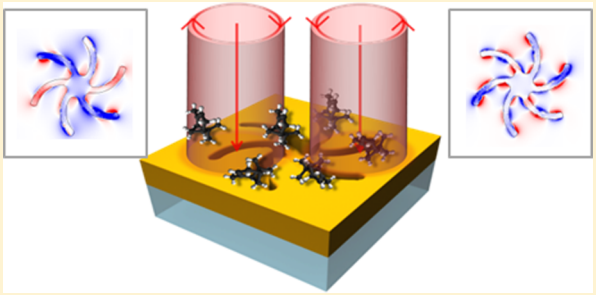

KEYWORDS: *chiral plasmonics, plasmonic induced transparency*

Light can be manipulated in unique ways with artificially engineered metamaterials, which are composed of nanostructures with dimensions comparable to the wavelength of light. The new phenomena offered by these materials lay the foundations for disruptive sensing, data storage, and photovoltaic technologies.[1−3] The optical responses of metamaterials are defined by the nanostructure properties governed by the interaction between the individual constituent elements.[4] The accepted paradigm for controlling optical properties is to manipulate coupling between nanostructure elements through the use of shape and symmetry. This geometry-driven design philosophy is inherently limited as optical properties are for the most part predetermined, with little scope for postfabrication tuning.

Here we present a new phenomenon by which coupling between nanostructure elements can be manipulated, and thus, the optical properties of metamaterials controlled. We show that in chiral metamaterials, coupling between optically bright and dark chiral modes can be controlled by manipulating the chiral asymmetries of the near fields. Thus, by controlling the chiral asymmetries of the nearfield either by the choice of incident polarization or the handedness of a surrounding chiral dielectric, coupling between bright and dark modes and thus optical properties can be manipulated. Put simply, the chiral nearfield has an asymmetric interaction with chiral plasmonic modes, which can be used to control coupling between chiral states. The concept is analogous to the asymmetry in the interaction of circularly polarized light (CPL) with chiral molecular electronic states. This is a new concept for the metamaterial design toolbox, which we refer to as "dichroic coupling", that provides a strategy for the rational design of functional hybrid molecular-plasmonic chiroptical materials for application in biosensing and polarization control.

We utilize dichroic coupling to control plasmonic metamaterial transparency. Metamaterials exhibit an analogue of the quantum interference phenomenon known as electromagnetic induced transparency (EIT), which is observed in atomic systems; it is the result of strong near-field coupling between bright and dark modes.[5−7] Controlling the coupling allows tuning of the optical properties of the coupled system that can be exploited in practical applications such as modulation of dispersion and group velocity, creating broadband delay lines, cryptography, communications, and biosensing.[8−10] The phenomenon we observe has more recently been referred to as electromagnetic induced reflectance (EIR).[11,12] However, in some of the earlier reported observations of the phenomenon, it was referred to as EIT.[5,13] For consistency, we will refer to the phenomenon as EIT(EIR). Most importantly, the underlying physics of both EIT and EIR in plasmonic systems is identical. EIT(EIR) has been observed in complex metamaterials that consist either of multiple structural elements (e.g.,

Received: September 15, 2017
Published: November 10, 2017

DOI: 10.1021/acsphotonics.7b01071
ACS Photonics 2018, 5, 535−543

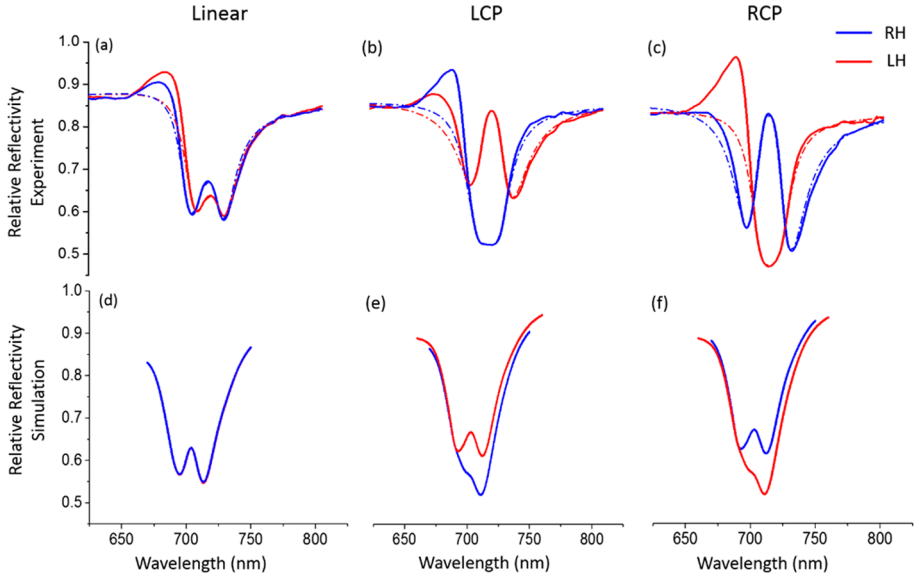

Figure 1. Reflectivity spectra for RH and LH shuriken nanostructures in water. Experimental data (solid lines) and curves fitted by the plasmonic EIT(EIR) model (dashed lines) are included for (a) linearly polarized input light, (b) LCP and (c) RCP. Equivalent reflectivity from electromagnetic simulations are included for (d) linear, (e) LCP, and (f) RCP. Note that the simulation data for linear polarization does show both LH and RH structures, but they overlap completely.

dolmen structures) or a single structure with high levels of rotational symmetry.[5,14−16] Such structures provide bright and dark modes that can spatially overlap and facilitate coupling. In previous work, the coupling between bright and dark modes, and thus the extent of EIT(EIR), was enhanced or reduced through changing geometry.[17−19] It has been reported that the level of EIT(EIR) in a 3-D chiral metamaterial excited by circularly polarized light can be manipulated by changing the degree of symmetry breaking by altering the geometry of the structure.[20] In this study we demonstrate the ability to control the EIT(EIR) behavior of a chiral plasmonic metamaterial by manipulating the chiral asymmetries of the near fields.

Fundamental to our dichroic coupling hypothesis is that near fields can have an intrinsic chiral asymmetry; this has been both theoretically predicted and experimentally demonstrated.[21,22] An optical chirality factor (C; Supporting Information 3.2) is used to parametrize the chiral asymmetries of near fields. In certain regions of space, near fields can exhibit C greater than that of CPL of equivalent frequency and are referred to as being superchiral. Asymmetry in the excitation of a chiral state by left handed (LH) and right handed (RH) superchiral fields will be larger than that for CPL. For the chiral field, which is generated by the optical excitation of the chiral bright mode, we propose that its coupling to the chiral dark mode is dependent on the C of the near field. Specifically, LH (RH) superchiral fields generated by the optical excitation of a bright mode will interact more strongly with a LH (RH) dark mode; thus increasing coupling.

RESULTS

In this study we have used chiral plasmonic gold metafilms that sustain both bright (dipole) and dark (quadrupole) modes.[16,23] The metafilms are fabricated by depositing gold on nanopatterned polycarbonate templates, henceforth referred to as templated plasmonic substrates (TPS).[24] The TPS consist of "shuriken"-shaped indentations, with 6-fold rotational symmetry, of either left-handedness (LH) or right-handedness (RH), arranged in a square lattice (further details in Supporting Information 1.1).

Effects of Incident Polarization. Figure 1a−c shows the reflectance spectra collected from LH(RH) substrates measured by monitoring scattered linearly polarized light and LH and RH CPL. The reflectance spectra show dependency on both the handedness of the structure and the helicity of the light. When the handedness of the structure and helicity of light match, the reflectance spectra display a region of enhanced reflectivity characteristic of EIT(EIR). In contrast, when helicity and structure are mismatched, the region of transparency is absent. The spectra collected with linear polarized light are intermediate between the two cases, which is consistent with the fact that linearly polarized light can be considered a 50:50 combination of LH and RH CPL. Initially the mismatched spectra appear to have Fano-like profiles. However, although the Fano function can replicate the bisignate nature of the reflectivity dips in the mismatched spectra, overall it provides a poor fit (see Supporting Information 4.2). Thus, we propose that the observed profiles are governed by coupling, albeit to varying degrees, between bright and dark modes. However, resonant scattering from this process undergoes interference with a scattered background causing a convolution with a Fano line shape.

To assess the level of coupling between bright and dark modes for each structure/light polarization combination, we fit the reflectance profiles using a simple classical model to describe plasmonic EIT(EIR). To simplify the fitting procedure and to prevent the possibility of overfitting, we neglect any Fano character of the reflectance dip profile. The model is based on two coupled oscillators and replicates reflectance spectra well, validating the neglect of Fano character. Variations of this approach have been used in a number of studies.[7,25] The starting point is a model system that is described by a set of two coupled harmonic oscillators,

$$\omega_r^{-2}\ddot{p}(t) + \gamma_r\omega_r^{-1}\dot{p}(t) + \dot{p}(t) = gf(t) - \tilde{\kappa}q(t) \quad (1)$$

DOI: 10.1021/acsphotonics.7b01071
ACS Photonics 2018, 5, 535−543

$$\omega_d^{-2}\ddot{q}(t) + \gamma_d\omega_d^{-1}\dot{q}(t) + q(t) = -\tilde{\kappa}p(t) \quad (2)$$

The radiative (bright) resonator is described by the excitation $p(t)$ with a resonance frequency ω_r and damping factor γ_r. Similarly, the dark mode excitation is described by $q(t)$ with a resonance frequency ω_d and damping factor γ_d. The two resonators are coupled via a coupling constant κ. The bright mode is driven by an external force $f(t)$ and g is a constant indicating the coupling strength between the oscillator and the external force. Unlike previous applications of the coupled oscillator model to plasmonic transparency, we include terms $e^{i\theta}$ and $e^{i\phi}$, which account for retardation phase shifts, θ and ϕ, in the bright and dark mode excitations, respectively. Both resonators are then coupled via a complex coupling coefficient $\tilde{\kappa} = \kappa e^{-i(\theta-\phi)}$. The solutions of (1) and (2) take the form

$$p(t) = e^{-i\theta}P(\omega)e^{-i(\omega t)} \quad (3)$$

$$q(t) = e^{-i\phi}Q(\omega)e^{-i(\omega t)} \quad (4)$$

Assuming an effective medium approximation and using the above equations, an expression for the reflectivity can be derived and used for fitting the experimental data. A full description of the fitting procedure and a complete list of the parameters required to fit the spectra are given in Supporting Information 4.1 and 5.1.

The coupling constants (κ) derived from fitting the experimental reflectance profiles, Figure 1a–c, are given in Table 1. The coupling constants for the matched combinations

Table 1. Coupling Constants from Plasmonic EIT Model[a]

coupling (κ) × 10^{-2}	LCP	linear	RCP
LH	4.8 ± 0.1	3.6 ± 0.1	2.6 ± 0.1
RH	2.8 ± 0.1	3.9 ± 0.1	5.1 ± 0.1

[a]This data is extracted by fitting the experimental data in Figure 1.

are approximately a factor of 2 larger than those of the mismatched. While, as would be expected, the values obtained for linear polarization are approximately half way in between those of the matched and mismatched.

Simulating the Effects of Polarization. To both validate our experimental measurements and to test the central hypothesis of our work, coupling between chiral bright and dark modes is governed by the chirality of the near fields, EM simulations have been performed. We obtain the reflectance spectra for the structure-polarization combinations measured, Figure 1d–f. There is very good agreement between the simulated and the experimental reflectance spectra for linear polarized light. For CPL there is qualitative agreement between experiment and simulated spectra. The presence (absence) of the transparency dip in the matched (mismatched) structure–polarization combinations are reproduced. However, the simulations underestimate the size of the transparency dip in the matched combinations, which implies an underestimate of the level of coupling between bright and dark modes owing to our interpretation of the experimental results. We speculate that geometrical differences between the fabricated and simulated structures, such as sloping of the edges or the arm curvature that introduce additional symmetry breaking to the structure, as previously demonstrated, may be the reason for this.[26] Thus, it may be the case that such geometric properties change the extent of the EIT(EIR) effect.

The optical chirality parameter C has been used to parametrize the level of chiral asymmetry of the near fields and is normalized to the value of that of CPL.[21,27] The simulated spatial distribution of the C of the near fields for structure–polarization combinations are shown in Figure 2 (a–f top surface, g–l bottom surface). The C of the nearfield is dependent on both the incident light polarization and the handedness of the structure. It is clear that regions of the near fields exhibit magnitudes of C greater than that of CPL (>1, i.e., are superchiral), with magnitudes of around 10 at the bottom surface of the structure and up to 100 at the top surface. The scale bars shown in Figure 2 are ranged manually to aid comparison of the top and bottom surfaces. In order to visually see the regions of minimum optical chirality, the scale bar values are reduced, hence, the regions showing large chirality values show saturation. See Supporting Information 8.3 for maximum scales. The structures also generate nearfields of both handedness (positive for LH and negative for RH), albeit one in excess. It should be noted that the C distributions for circularly polarized light (i.e., Figure 2b,c,e,f and h,i,k,l) exhibit 2-fold rotational symmetry rather than the 6-fold rotational symmetry that might have been expected. The explanation for this is the symmetry reduction caused by the shurikens being arranged in a periodic square lattice, as the unit cell of this structure has only 2-fold rotational symmetry. Simulations for an isolated shuriken structure display the expected 6-fold rotational symmetry (see Supporting Information 8.1).

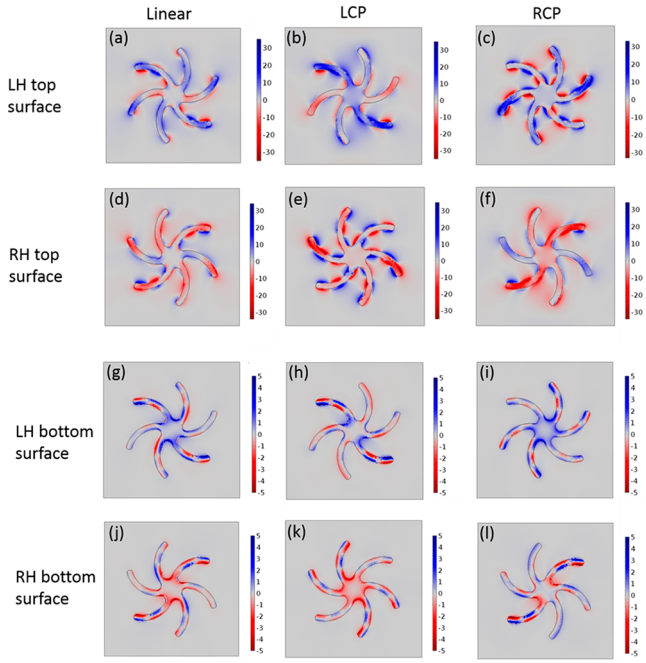

Figure 2. Data obtained from simulations of hybrid shuriken structures in water. The spatial distribution of chirality factor C for each combination in Figure 1 is shown for (a)–(f) the hybrid structure top surface and (g)–(l) the hybrid structure bottom surface.

The C value can vary depending on the wavelength position examined, in particular when calculated at the left peak, central dip or right peak of the EIT(EIR) response (Supporting Information 8.2). From the maps it is clear that the sign of the net optical chirality does not change in the region spanning the left peak, central dip and right peak. In contrast, for the

DOI: 10.1021/acsphotonics.7b01071
ACS Photonics 2018, 5, 535–543

matched and linear cases, the spatial distribution of optical chirality shows a dramatic change around the EIT(EIR) window, indicative of strong coupling to the dark mode for these combinations.

Based on the dichroic coupling hypothesis it can be assumed that for LH (RH) structures the level of coupling is governed by the magnitude of the C values for LH (RH) chiral near fields. Hence, the highest level of coupling for LH (RH) would occur for nearfields which have the highest level of LH(RH) chiral asymmetry, that is, they have the most positive (negative) value of optical chirality. Consequently, we define a parameter C_{max} that is the maximum positive (negative) value for the nearfield for LH (RH) structures.

In Figure 3, the coupling constants derived from fitting the experimental data with the classical coupled oscillator model

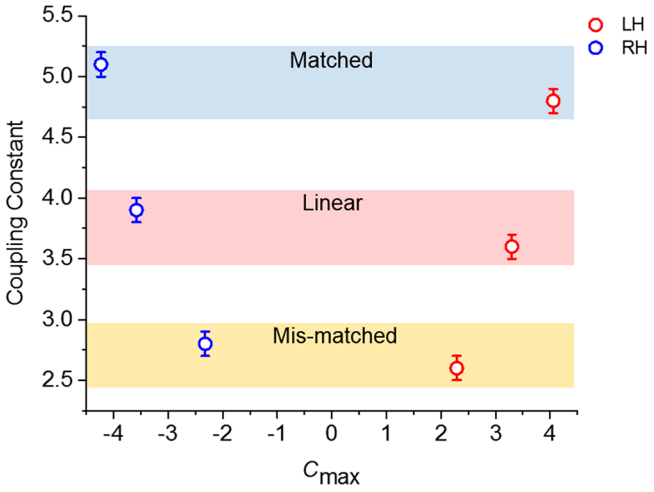

Figure 3. Effect of chirality on near-field coupling in the nanostructures. The coupling constants for each structure−polarization combination are taken from Table 1, and the C_{max} values were calculated from simulation data for the observed points of highest chirality.

are plotted against C_{max}. Consistent with our hypothesis coupling scales with optical chirality; with matched and mismatched combinations generating nearfields with the highest and lowest levels of C_{max}, respectively.

The data presented provides prima facie evidence of the validity of our dichroic coupling hypothesis through presenting a correlation between coupling and the optical chirality of the near fields. For an unambiguous validation, we provide further evidence that the plasmonic transparency, and hence bright-dark mode coupling, is correlated to the chiral asymmetry of the near field. Specifically, we will show that optical chirality of the nearfields can be manipulated (i.e., increase or decrease systematically) by the introduction, around the nanostructure, of a (isotropic) chiral dielectric.

Simulating the Effects of Isotropic Chiral Dielectrics. We first present EM simulations which demonstrate that introducing an isotropic chiral dielectric both increases the C_{max} and also increases the coupling, between bright and dark modes, changing the plasmonic transparency behavior of the substrate. Simulations are focused on linearly polarized light. The isotropic chiral dielectric is modeled using the constitutive equations for a chiral medium:

$$D = \varepsilon_0 \varepsilon_r E + i\xi B \tag{5}$$

$$H = B/\mu + i\xi E \tag{6}$$

Here, ε_0 is the permittivity of free space, ε_r is the relative permittivity, μ is the permeability, E is the complex electric field, B is the complex magnetic flux density, H is the magnetic field, D is the electric displacement field, and ξ is a local parameter describing the chiral property of a molecular layer. ξ is only nonzero for a chiral dielectric. The sign of ξ is defined by the handedness of the chiral dielectric and its value can be estimated using the general form given by[28]

$$\xi = \beta_c \left(\frac{1}{\hbar\omega + \hbar\omega_0 + i\Gamma_{12}} + \frac{1}{\hbar\omega - \hbar\omega_0 + i\Gamma_{12}} \right) \tag{7}$$

The parameters in eq 7 can be estimated from the quantum equation of motion of density matrix assuming a low density of molecules as described by Govorov et al.[28] Here β_c is an intrinsic coefficient that determines the magnitude of chiral properties and we use $\beta_c = 4.1 \times 10^{-4}$. Here $\hbar\omega_0$ (where $\hbar$ is the reduced Planck's constant $h/2\pi$ and ω_0 is the absorption frequency) and Γ are the energy and intrinsic width of the resonant chiral excitation of the dielectric. Consequently, the value of ξ at a particular wavelength is dependent on the chiroptical properties of the chiral dielectric. Chiral organic molecules tend to have absorption near the far UV region and corresponding ξ values (at ∼700 nm) lie at around 4×10^{-5}, see Supporting Information 6.1. In order to observe the effects of ξ on the plasmonic response of the chiral nanostructure, simulations are performed for $0 < \xi < 1.5 \times 10^{-4}$.

We wish to compare the level of coupling predicted by modeling with that observed experimentally. In this case, we have chosen not to compare κ values, as we did for the effects of CPL, but have instead used a simpler parameter, separation (S) of the two minima either side of the reflectivity dip. From the coupled oscillator model it is apparent that S is dependent on the coupling constant κ (see Supporting Information 4.1). In contrast to CPL data, and the mismatched combination in particular, all linearly polarized data show reflectance dips; therefore, S values can be obtained for all data sets. The S value can also be measured more accurately from both experiment and simulation, than the κ value derived from fitting both sets of data, which is the principle motivation for its choice. To parametrize the asymmetry of the effects of chiral dielectrics on the reflectance spectra, hence, asymmetry in κ, we derive a parameter from S:

$$\Delta\Delta S = ({}^{\text{chiral}}S_{RH} - {}^{\text{water}}S_{RH}) - ({}^{\text{chiral}}S_{LH} - {}^{\text{water}}S_{LH})$$

where ${}^{\text{chiral/water}}S_{LH/RH}$ is the separation of the reflectance dips for LH(RH) structures in the presence of water (chiral dielectric). Thus, $\Delta\Delta S$ parametrizes the asymmetry in κ induced by the presence of a chiral dielectric.

In Figure 4a,b are the results for simulations with linearly polarized light for varying magnitudes of positive ξ. Two significant conclusions can be drawn from the simulated spectra. First, for the RH structure, the presence of a chiral dielectric enhances the coupling between bright and dark modes, leading to an increase in the wavelength range over which the transparency window occurs; and this effect increases with ξ. Second, the effect of the chiral dielectric is asymmetric, with a reduction in the coupling for the LH structure, hence, showing a differential change in the separation/coupling; the size of the asymmetry increases with increasing ξ, Figure 4c.

DOI: 10.1021/acsphotonics.7b01071
ACS Photonics 2018, 5, 535−543

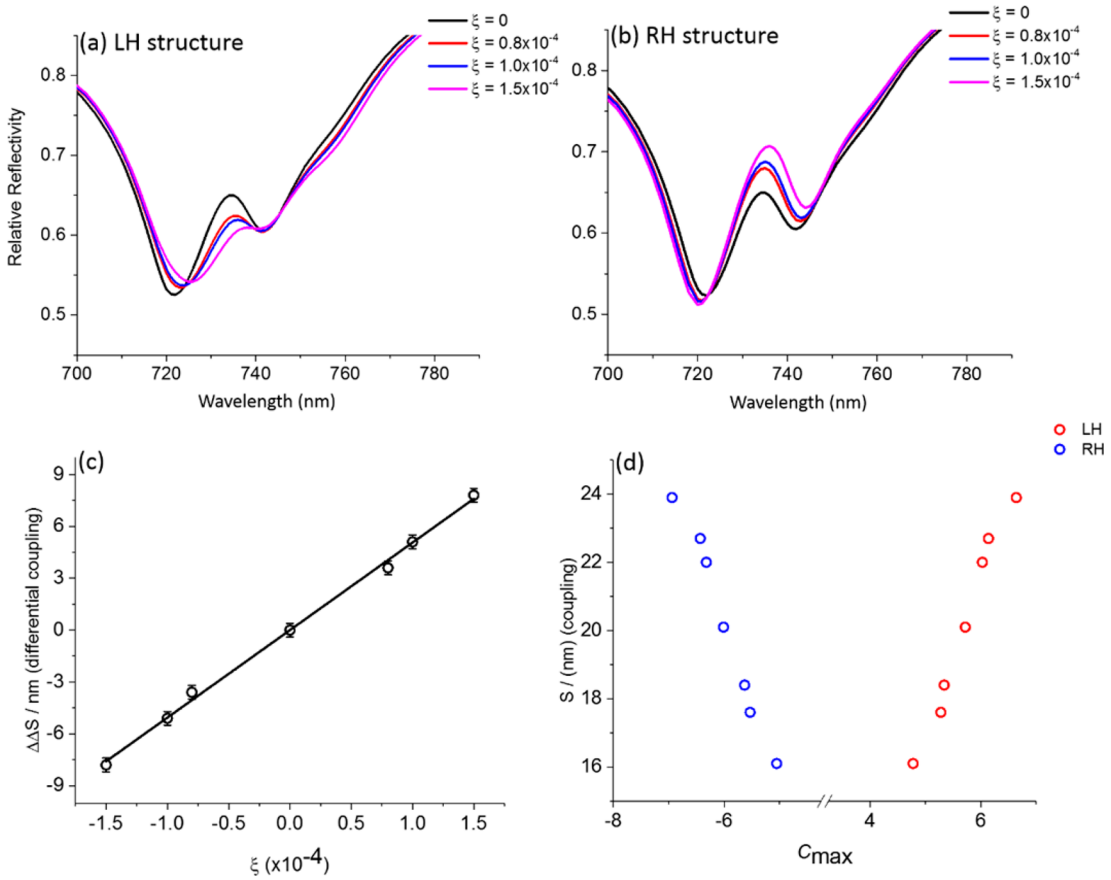

Figure 4. Effects of ξ value on S and relation to chirality. Simulated spectra of isotropic chiral liquid layers on shurikens are given for (a) LH structures and (b) RH structures over a range of positive ξ values. The $\Delta\Delta S$ values for these spectra are then plotted against ξ in (c). The S values are also extracted from the simulated spectra and plotted against C_{max} at the bottom surface in (d).

As expected the level of coupling is correlated to the C_{max} of the nearfield; a plot of S versus C_{max} is shown in Figure 4d. Introducing a positive ξ chiral dielectric causes an increase in C_{max} for the RH, but reduces it for LH structures. Thus, coupling in the RH (LH) case becomes enhanced (reduced) because the chiral asymmetry of the nearfield increases (decreases).

It is important to note that both EM simulations and experimental measurements demonstrate that both the level of coupling and optical chirality are not affected by small changes in properties of an achiral dielectric (altering the refractive index from 1.33 to 1.344 see Supporting Information 5.2). However, the level of coupling for higher refractive index ($\geq$1.4) dielectrics is higher than that of water owing to the fact that the quadrupole mode has a slightly larger refractive index sensitivity than the dipole mode. Consequently, the change in the relative position of the two modes becomes significant at higher refractive index causing an increase in coupling. This effect is independent of chirality and is replicated in simulations.

Experimental Verification. To confirm the prediction of the EM simulations we have performed experiments using chiral dielectrics that display a range of ξ values. Three isotropic chiral liquids have been studied, namely (+)- and (−)-α-pinene as well as a racemic mixture of the two. We have also deposited a 20 nm thick polycrystalline film of chlorophyll a (circular dichroism spectrum shown in Supporting Information 7.1) onto the substrates. The motivation for the choice of these materials is that the pinenes allow both enantiomers and a racemic mixture to be studied, while chlorophyll would be expected to have a ξ value significantly larger in magnitude than those of the pinene enantiomers. This is because pinenes display CD in the UV, whereas chlorophyll a displays CD in the VIS spectrum.[29,30] Thus, based on eq 7, chlorophyll a would be expected to have a larger ξ value.

Figure 5 shows the reflectance spectra collected from LH and RH structures in the presence of the chiral dielectric media. The experimentally derived $\Delta\Delta S$ values for the pinenes and chlorophyll a can be replicated with simulations, Figure 6, assuming a refractive index of 1.4 for pinene and 1.34 for chlorophyll, as well as ξ values of 2.6×10^{-5} and 3×10^{-4} that are close to those expected using eq 7, $\sim 4 \times 10^{-5}$ and $\sim 3 \times 10^{-4}$, respectively. Although chlorophyll a and pinenes induce similar levels of asymmetries, for the former case, this is achieved using a 20 nm film rather than a complete chiral environment. This is consistent with the larger ξ value of chlorophyll a.

The asymmetries in separation values ($\Delta\Delta S$) for experimental and simulated results, as well as the matching ξ values are listed in Table 2.

DISCUSSION

The essence of the dichroic coupling hypothesis is that chiral nearfields interact asymmetrically with plasmonic resonances; in an analogous manner to the asymmetric interaction of CPL with chiral electronic molecular states. In the current study,

DOI: 10.1021/acsphotonics.7b01071
ACS Photonics 2018, 5, 535−543

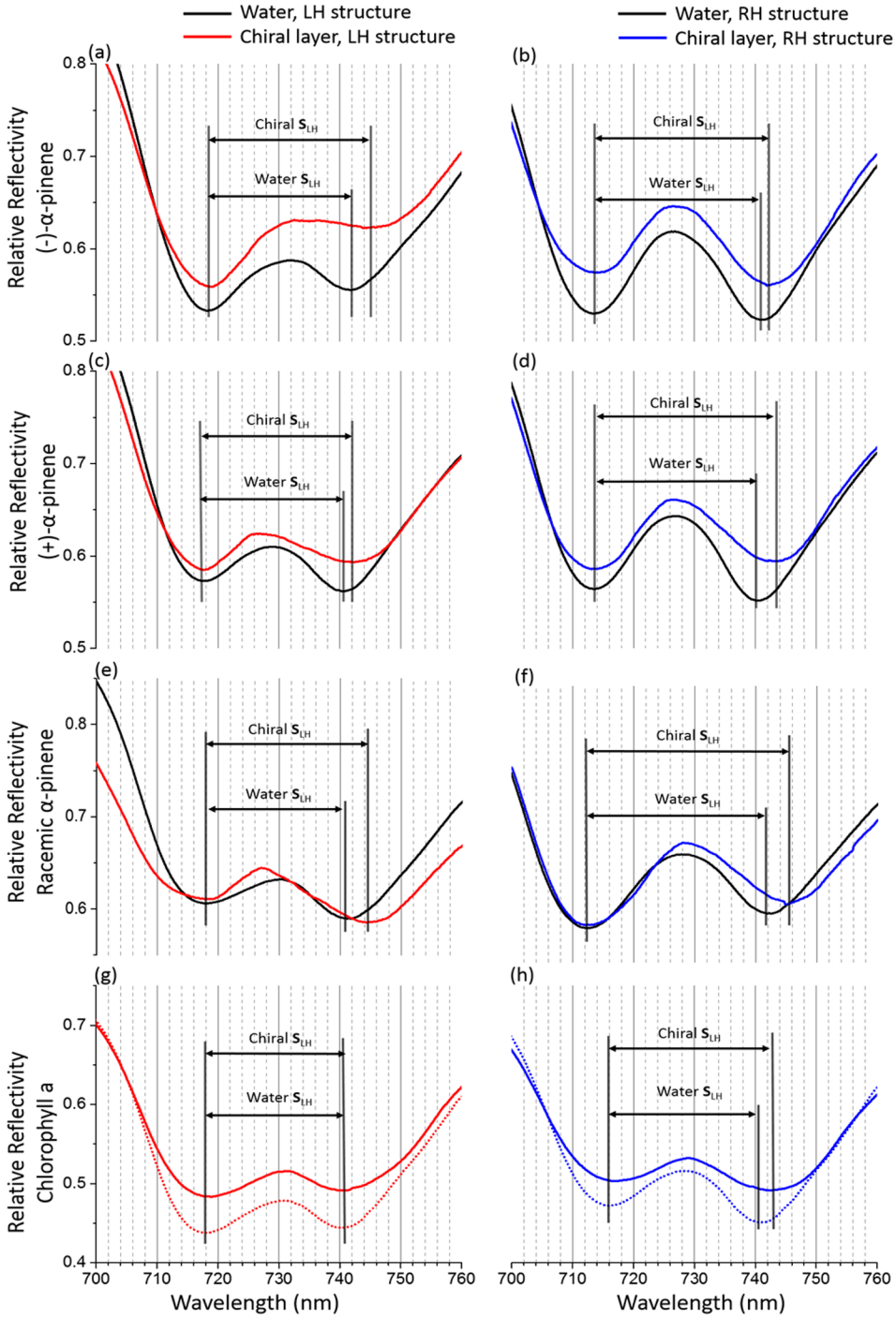

Figure 5. Experimental reflectivity in water (black) and chiral material is shown for (a, b) (−)-α-pinene, (c, d) (+)-α-pinene, (e, f) racemic α-pinene, and (g, h) chlorophyll a. Red lines are used for the LH structures and blue for the RH. The chiral spectra have been horizontally shifted to overlap with water to aid comparison.

chiral near fields generated by the excitation of a chiral (bright) dipole mode, display asymmetric interaction, (i.e., dependent on the handedness of the near field) with a chiral (dark) quadrupole mode. The asymmetry of the interaction of the chiral nearfield controls the coupling between the dark and bright modes, and hence plasmonic transparency. Thus, coupling in such resonator systems can be controlled by manipulating the chirality of the near fields. This was achieved by using both the polarization of the incident light and by the introduction of chiral dielectrics. The level to which a chiral dielectric can change the optical chirality of the near field is determined by its chiroptical properties.

An important observation of this study is the large magnitude of the dichroic coupling, changes of ∼50% are observed in κ when the handedness of the nearfields are switched by using CPL. Since κ is determined by the excitation of the chiral (dark) quadrupole mode by the chiral nearfield, this implies an asymmetry factor of 50%. This level of asymmetry in the interaction of chiral near fields with a chiral quadrupole mode is greater by 3 orders of magnitude than that displayed in the excitation of chiral molecular resonances by CPL. This

DOI: 10.1021/acsphotonics.7b01071
ACS Photonics 2018, 5, 535−543

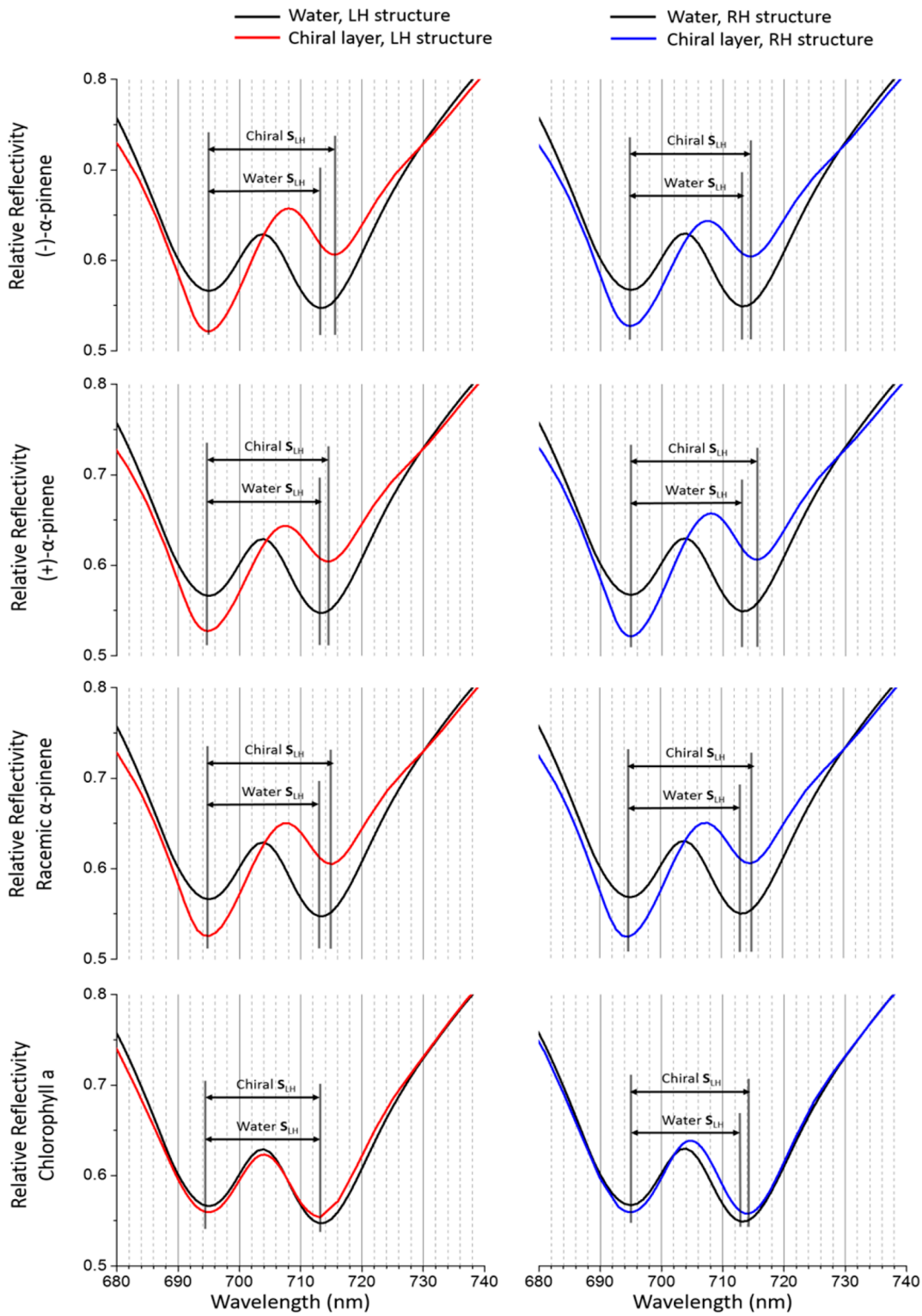

Figure 6. Simulation data using a refractive index of 1.4 for pinenes and 1.34 for chlorophyll. Reflectivity in water (black lines) and chiral medium is shown for (a, b) (−)-*α*-pinene, (c, d) (+)-*α*-pinene, (e, f) racemic *α*-pinene, and (g, h) chlorophyll a. Red lines are used for the LH structures and blue for the RH. As in Figure 5, the plots for chiral media have been horizontally shifted to overlap with water to aid comparison.

difference in magnitude of the asymmetry factor can only partially be attributed to the superchirality of the near field (1−2 orders of magnitude). This implies an inherently higher level of asymmetry in the interaction of chiral near fields with chiral plasmonic (quadrupole) modes. Such a conclusion is supported by work by Jain et al. which shows that nondipole transitions which are forbidden in the farfield are allowed with nearfields.[31] We suggest that this concept can be extended to the enhanced asymmetry in excitations of chiral dark modes by chiral nearfields.

Our proposal of a dichroic coupling model provides a foundation for understanding how chiral dielectric materials can

DOI: 10.1021/acsphotonics.7b01071
ACS Photonics 2018, 5, 535−543

Table 2. Experimentally Obtained $\Delta\Delta S$ Values for the Various Chiral Layers That Were Investigated and Those Obtained from the Corresponding Simulations[a]

	(−)-α-pinene	(+)-α-pinene	racemic α-pinene	chlorophyll a
$\Delta\Delta S$ (nm) experiment	−1.4 ± 0.3	1.2 ± 0.3	0.1 ± 0.3	1.0 ± 0.3
$\Delta\Delta S$ (nm) simulation	−1.3 ± 0.3	1.3 ± 0.3	0.0 ± 0.3	1.1 ± 0.3
ξ calcd	-4.0×10^{-5}	4.0×10^{-5}	0.0	3.0×10^{-4}
ξ in simulation	-2.6×10^{-5}	2.6×10^{-5}	0.0	3.0×10^{-4}

[a]Included are approximate the values of ξ calculated using eq 7 as well as those values used in the simulations.

influence the optical properties of chiral plasmonic metamaterials. In previous studies, superchiral fields have been shown to be sensitive to chiral structure of (bio)materials over a range of length scales. A "polarimetry" model was used to rationalize the results of these studies, in which the ability of a chiral molecule to induce asymmetric behavior in optical properties of LH and RH chiral plasmonic metamaterials was assigned to a large asymmetry in the effective refractive index of a chiral layer in chiral near field.[32] However, theoretical work could not replicate the magnitude of the effects observed.[33] Our work shows that the ability of chiral media to induce asymmetric behavior is more complex than the "polarimetry" model and that it is the ability of chiral dielectrics to alter plasmonic coupling that is the origin of the observed effects.

In summary, we demonstrate an intuitive dichroic coupling model, based on large dissymmetry in the interactions of chiral nearfields with chiral multipole modes. By tuning the optical chirality of the nearfields, coupling between chiral dipole and multipole modes can be controlled, and thus plasmonic transparency manipulated. In this study CPL and isotropic chiral dielectrics have been used to control the optical chirality of the nearfield. However, using incident optical beam with exotic polarization states to achieve enhanced optical chirality in the near field,[34] or anisotropic chiral liquid crystal phases (which have largest effective ξ values available for molecular materials),[35] would provide even greater changes on nearfield optical chirality and hence metamaterial transparency. Thus, our work provides a valuable new concept for the metamaterial toolbox that both enables design optimization and a rational basis for analytical applications in biomaterials/soft matter.

■ ASSOCIATED CONTENT

Supporting Information

The Supporting Information is available free of charge on the ACS Publications website at DOI: 10.1021/acsphotonics.7b01071.

Materials and methods, nanostructure description, electromagnetic simulations, EIT mathematical model, experimental and fitting results, calculations of ξ, circular dichroism of chlorophyll a, and additional information for optical chirality plots (PDF).

■ AUTHOR INFORMATION

Corresponding Authors

*E-mail: malcolm.kadodwala@glasgow.ac.uk.
*E-mail: affar.karimullah@glasgow.ac.uk.
*E-mail: c.kelly.4@research.gla.ac.uk.

ORCID

Nikolaj Gadegaard: 0000-0002-3396-846X
Alexander O. Govorov: 0000-0003-1316-6758
Affar S. Karimullah: 0000-0002-8792-9829

Notes

The authors declare no competing financial interest.

■ ACKNOWLEDGMENTS

The authors acknowledge financial support from the Engineering and Physical Sciences Research Council (EP/K034936/1), National Science Foundation (NSF Grant CHE-1307021), JSPS Core to Core (EP/M024423/1), and the technical support from the James Watt Nanofabrication Centre (JWNC). C.K. thanks the Carnegie Trust for the award of a Ph.D. scholarship.

■ REFERENCES

(1) Atwater, H. a; Polman, A. Plasmonics for Improved Photovoltaic Devices. *Nat. Mater.* **2010**, *9*, 205−213.
(2) Anker, J. N.; Hall, W. P.; Lyandres, O.; Shah, N. C.; Zhao, J.; Van Duyne, R. P. Biosensing with Plasmonic Nanosensors. *Nat. Mater.* **2008**, *7*, 442−453.
(3) Zhang, J.; Gecevi, M.; Beresna, M.; Kazansky, P. G. Seemingly Unlimited Lifetime Data Storage in Nanostructured Glass. *Phys. Rev. Lett.* **2014**, *112*, 1−5.
(4) Liu, N.; Giessen, H. Coupling Effects in Optical Metamaterials. *Angew. Chem., Int. Ed.* **2010**, *49*, 9838−9852.
(5) Liu, N.; Langguth, L.; Weiss, T.; Kästel, J.; Fleischhauer, M.; Pfau, T.; Giessen, H. Plasmonic Analogue of Electromagnetically Induced Transparency at the Drude Damping Limit. *Nat. Mater.* **2009**, *8*, 758−762.
(6) Luk'yanchuk, B.; Zheludev, N. I.; Maier, S. A.; Halas, N. J.; Nordlander, P.; Giessen, H.; Chong, C. T. The Fano Resonance in Plasmonic Nanostructures and Metamaterials. *Nat. Mater.* **2010**, *9*, 707−715.
(7) Zhang, S.; Genov, D. a.; Wang, Y.; Liu, M.; Zhang, X. Plasmon-Induced Transparency in Metamaterials. *Phys. Rev. Lett.* **2008**, *101*, 47401.
(8) Wu, C.; Khanikaev, A. B.; Adato, R.; Arju, N.; Yanik, A. A.; Altug, H.; Shvets, G. Fano-Resonant Asymmetric Metamaterials for Ultrasensitive Spectroscopy and Identification of Molecular Monolayers. *Nat. Mater.* **2011**, *11*, 69−75.
(9) Gu, J.; Singh, R.; Liu, X.; Zhang, X.; Ma, Y.; Zhang, S.; Maier, S. A.; Tian, Z.; Azad, A. K.; Chen, H.; Taylor, A. J.; Han, J.; Zhang, W. Active Control of Electromagnetically Induced Transparency Analogue in Terahertz Metamaterials. *Nat. Commun.* **2012**, *3*, 1151.
(10) Wu, C.; Khanikaev, A. B.; Shvets, G. Broadband Slow Light Metamaterial Based on a Double-Continuum Fano Resonance. *Phys. Rev. Lett.* **2011**, *106*, 107403.
(11) Vafapour, Z.; Zakery, A. New Approach of Plasmonically Induced Reflectance in a Planar Metamaterial for Plasmonic Sensing Applications. *Plasmonics* **2016**, *11*, 609−618.
(12) Vafapour, Z. Near Infrared Biosensor Based on Classical Electromagnetically Induced Reflectance (Cl-EIR) in a Planar Complementary Metamaterial. *Opt. Commun.* **2017**, *387*, 1−11.
(13) Liu, N.; Weiss, T.; Mesch, M.; Langguth, L.; Eigenthaler, U.; Hirscher, M.; Sönnichsen, C.; Giessen, H. Planar Metamaterial Analogue of Electromagnetically Induced Transparency for Plasmonic Sensing. *Nano Lett.* **2010**, *10*, 1103−1107.
(14) Liu, N.; Liu, H.; Zhu, S.; Giessen, H. Stereometamaterials. *Nat. Photonics* **2009**, *3*, 157−162.
(15) McNamara, H. M.; Zhang, H.; Werley, C. A.; Cohen, A. E. Optically Controlled Oscillators in an Engineered Bioelectric Tissue. *Phys. Rev. X* **2016**, *6*, 31001.
(16) Karimullah, A. S.; Jack, C.; Tullius, R.; Rotello, V. M.; Cooke, G.; Gadegaard, N.; Barron, L. D.; Kadodwala, M. Disposable

DOI: 10.1021/acsphotonics.7b01071
ACS Photonics 2018, 5, 535−543

Plasmonics: Plastic Templated Plasmonic Metamaterials with Tunable Chirality. *Adv. Mater.* **2015**, *27*, 5610−5616.
(17) Hentschel, M.; Weiss, T.; Bagheri, S.; Giessen, H. Babinet to the Half: Coupling of Solid and Inverse Plasmonic Structures. *Nano Lett.* **2013**, *13*, 4428−4433.
(18) Schäferling, M.; Engheta, N.; Giessen, H.; Weiss, T. Reducing the Complexity: Enantioselective Chiral Near-Fields by Diagonal Slit and Mirror Configuration. *ACS Photonics* **2016**, *3*, 1076−1084.
(19) Liu, N.; Hentschel, M.; Weiss, T.; Alivisatos, A. P.; Giessen, H. Three-Dimensional Plasmon Rulers. *Science* **2011**, *332*, 1407−1410.
(20) Lin, H.; Yang, D.; Han, S.; Liu, Y.; Yang, H. Analog Electromagnetically Induced Transparency for Circularly Polarized Wave Using Three-Dimensional Chiral Metamaterials. *Opt. Express* **2016**, *24*, 30068.
(21) Tang, Y.; Cohen, A. E. Optical Chirality and Its Interaction with Matter. *Phys. Rev. Lett.* **2010**, *104*, 163901.
(22) Hendry, E.; Mikhaylovskiy, R. V.; Barron, L. D.; Kadodwala, M.; Davis, T. J. Chiral Electromagnetic Fields Generated by Arrays of Nanoslits. *Nano Lett.* **2012**, *12*, 3640−3644.
(23) Jack, C.; Karimullah, A. S.; Leyman, R.; Tullius, R.; Rotello, V. M.; Cooke, G.; Gadegaard, N.; Barron, L. D.; Kadodwala, M. Biomacromolecular Stereostructure Mediates Mode Hybridization in Chiral Plasmonic Nanostructures. *Nano Lett.* **2016**, *16*, 5806−5814.
(24) Gadegaard, N.; Mosler, S.; Larsen, N. B. Biomimetic Polymer Nanostructures by Injection Molding. *Macromol. Mater. Eng.* **2003**, *288*, 76−83.
(25) Tassin, P.; Zhang, L.; Zhao, R.; Jain, A.; Koschny, T.; Soukoulis, C. M. Electromagnetically Induced Transparency and Absorption in Metamaterials: The Radiating Two-Oscillator Model and Its Experimental Confirmation. *Phys. Rev. Lett.* **2012**, *109*, 187401.
(26) Roller, E. M.; Khorashad, L. K.; Fedoruk, M.; Schreiber, R.; Govorov, A. O.; Liedl, T. DNA-Assembled Nanoparticle Rings Exhibit Electric and Magnetic Resonances at Visible Frequencies. *Nano Lett.* **2015**, *15*, 1368−1373.
(27) Davis, T. J.; Hendry, E. Superchiral Electromagnetic Fields Created by Surface Plasmons in Nonchiral Metallic Nanostructures. *Phys. Rev. B: Condens. Matter Mater. Phys.* **2013**, *87*, 85405.
(28) Govorov, A. O.; Fan, Z. Theory of Chiral Plasmonic Nanostructures Comprising Metal Nanocrystals and Chiral Molecular Media. *ChemPhysChem* **2012**, *13*, 2551−2560.
(29) Greg Mitchell, B.; Kiefer, D. A. Chlorophyll α Specific Absorption and Fluorescence Excitation Spectra for Light-Limited Phytoplankton. *Deep-Sea Res., Part A* **1988**, *35*, 639−663.
(30) Kubala, D.; Drage, E. A.; Al-Faydhi, A. M. E.; Kočíšek, J.; Papp, P.; Matejčík, V.; Mach, P.; Urban, J.; Limão-Vieira, P.; Hoffmann, S. V.; Matejčík, Š.; Mason, N. J. Electron Impact Ionisation and UV Absorption Study of α- and β-Pinene. *Int. J. Mass Spectrom.* **2009**, *280*, 169−173.
(31) Jain, P. K.; Ghosh, D.; Baer, R.; Rabani, E.; Alivisatos, a. P. Near-Field Manipulation of Spectroscopic Selection Rules on the Nanoscale. *Proc. Natl. Acad. Sci. U. S. A.* **2012**, *109*, 8016−8019.
(32) Hendry, E.; Carpy, T.; Johnston, J.; Popland, M.; Mikhaylovskiy, R. V.; Lapthorn, A. J.; Kelly, S. M.; Barron, L. D.; Gadegaard, N.; Kadodwala, M. Ultrasensitive Detection and Characterization of Biomolecules Using Superchiral Fields. *Nat. Nanotechnol.* **2010**, *5*, 783−787.
(33) Hendry, E.; Mikhaylovskiy, R. V.; Barron, L. D.; Kadodwala, M.; Davis, T. J. Chiral Electromagnetic Fields Generated by Arrays of Nanoslits. *Nano Lett.* **2012**, *12*, 3640−3644.
(34) Kramer, C.; Schäferling, M.; Weiss, T.; Giessen, H.; Brixner, T. Analytic Optimization of Near-Field Optical Chirality Enhancement. *ACS Photonics* **2017**, *4*, 396−406.
(35) de Gennes, P. G.; Prost, J. *The Physics of Liquid Crystals*; Clarendon Press, 1993.

DOI: 10.1021/acsphotonics.7b01071
ACS Photonics 2018, 5, 535−543